JGR Solid Earth

RESEARCH ARTICLE
10.1029/2020JB019861

Basal Accretion Along the South Central Chilean Margin and Its Relationship to Great Earthquakes

N. L. Bangs[1], J. K. Morgan[2], A. M. Tréhu[3], E. Contreras-Reyes[4], A. F. Arnulf[1], S. Han[1], K. M. Olsen[1], and E. Zhang[3]

[1]Institute for Geophysics, University of Texas at Austin, Austin, TX, USA, [2]Department of Earth, Environmental, and Planetary Sciences, William Marsh Rice University, Houston, TX, USA, [3]College of Earth, Ocean, and Atmospheric Sciences, Oregon State University, Corvallis, OR, USA, [4]Departamento de Geofísica, Facultad de Ciencias Físicas y Matemáticas, Universidad de Chile, Santiago, Chile

Key Points:
- The south central Chilean margin grows primarily by basal accretion rather than frontal accretion processes common to many subduction zones
- Intermittent basal accretion processes along the Chilean margin allow large fractions of the trench sediment to subduct into the seismogenic zone
- The large subducting sediment volume maintains a smooth, shallow décollement capable of building large strains and causing great earthquakes

Supporting Information:
- Supporting Information S1

Correspondence to:
N. L. Bangs,
nathan@ig.utexas.edu

Citation:
Bangs, N. L., Morgan, J. K., Tréhu, A. M., Contreras-Reyes, E., Arnulf, A. F., Han, S., et al. (2020). Basal accretion along the south central Chilean margin and its relationship to great earthquakes. *Journal of Geophysical Research: Solid Earth*, *125*, e2020JB019861. https://doi.org/10.1029/2020JB019861

Received 25 MAR 2020
Accepted 12 OCT 2020
Accepted article online 15 OCT 2020

Abstract The south central Chilean margin regularly produces many of the world's largest earthquakes and tsunami, including the 2010 *Mw* 8.8 Maule and 1960 *Mw* 9.5 Valdivia events. In 2017, we acquired seismic reflection data along ~1,000 km of the margin using the R/V *Langseth*'s 15 km long receiver array and 108.2 l (6,600 in^3) seismic source to image structures associated with these ruptures. We focus on the Valdivia segment with the largest coseismic slip (~40 m). The outer 40 km of the forearc is an accretionary wedge constructed primarily of stacked sedimentary packages with irregular lengths and thicknesses and little along-strike continuity. Forearc structures indicate that the accretionary wedge grows primarily through basal accretion of the downgoing trench fill. The décollement propagates along a weak boundary near the top of the trench fill but occasionally branches downward into the underthrust sediment along bedding horizons, peeling off slices that are underplated to the forearc. The shallow décollement level and the rarity of underplating events allow most of the trench sediment to subduct. As a result, only ~30% of the incoming sediment has been accreted since the Early Pliocene. This implies that, on average, ~1 km of sediment must subduct beyond the outer forearc, an inference that is supported by our seismic images. We propose that the thickness and great downdip and along-strike extent of the underthrust layer, which separates the megathrust from the underlying roughness of the igneous ocean crust, ensures a smooth broad zone of strong coupling that generates the world's largest earthquakes and tsunami.

1. Introduction

In 1960, a ~1,000 km long segment of the south central Chilean margin between the Mocha fracture zone and the Chile triple junction (Figure 1) ruptured to produce the largest earthquake ever recorded on global seismic networks (*Mw* 9.5). The Valdivia earthquake ruptured beneath the slope, shelf, and coastline, with slip up to 40 m (Barrientos & Ward, 1990; Cifuentes, 1989; Moreno et al., 2009). This particularly large rupture also generated a deadly tsunami that propagated across the Pacific Ocean. Recent GPS surveys of the Chilean margin confirm that the areas of largest slip in 1960 are now nearly locked and are accumulating significant strain (Moreno et al., 2012). Historical records show a behavior of regular, great earthquakes along the Valdivia rupture segment with a recurrence interval of ~150 years (Cisternas et al., 2005; Melnick et al., 2009), which is consistent with strong coupling throughout much of the earthquake cycle.

Subduction zones with thick trench and/or abyssal plain sediment sections are well correlated with Earth's greatest earthquakes and tsunamis (Heuret et al., 2012; Scholl et al., 2015), and thicknesses >1 km may even be a requirement for the largest earthquakes (>*Mw* 9.0; Seno, 2017). Thick subducted sediments may lead to more uniform coupling along the megathrust because the subducting sediment covers igneous ocean crust roughness (Contreras-Reyes & Carrizo, 2011; Van Rijsingen et al., 2018; Wang & Bilek, 2011), resulting in a relatively smooth, homogeneous décollement (the megathrust fault) at the top of the underthrust section that can support high shear stress during interplate locking over a large surface (Ruff, 1989).

To first order, the south central Chilean margin fits the global pattern of associating thick incoming sediment in the trench and great tsunamigenic earthquakes (Scholl et al., 2015). However, certain characteristics of this margin differ from the typical model of thickly sedimented seismogenic margins. Subduction zones with thick (>1 km) sediment accumulations on the incoming plate usually grow by slicing off trench sediments and piling them into imbricate thrust stacks along the leading edge of the overriding plate to form

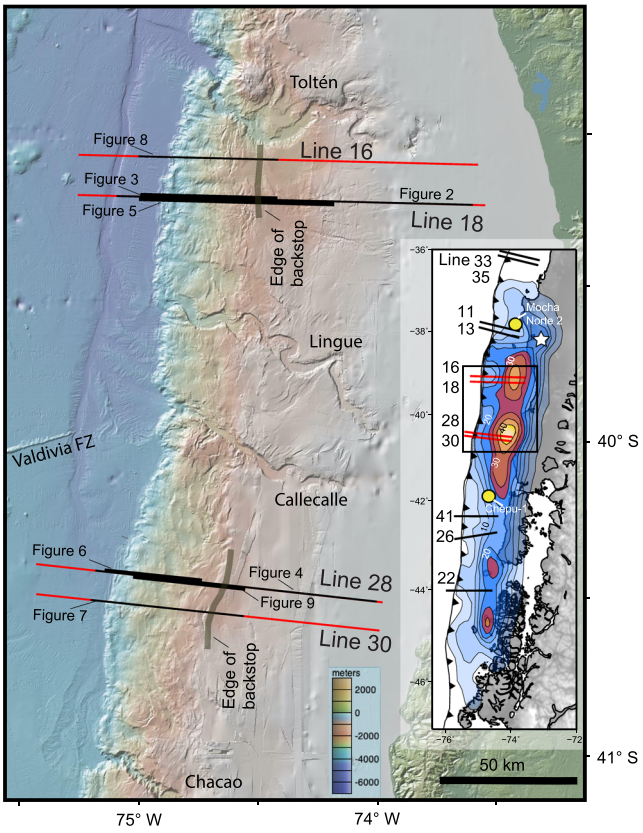

Figure 1. Bathymetry of the south central Chile margin within the 1960 Valdivia earthquake rupture area showing the track lines of four of the seismic reflection profiles acquired during the CEVICHE seismic imaging project. Inset shows the location of the bathymetry map (black rectangle) and the location of all of the margin perpendicular seismic lines from CEVICHE. The contours show slip estimated for the 1960 *Mw* 9.5 Valdivia earthquake (in meters) (Moreno et al., 2009). The star shows the location of the earthquake epicenter. The yellow circles are industry well locations from Gonzalez (1990). Valdivia FZ is the Valdivia fracture zone. Also labeled are the submarine canyons across the shelf and slope. Black line segments show the portions of the seismic lines shown in other figures.

large accretionary wedges (e.g., the Barbados, Westbrook, 1982; Nankai, Moore et al., 2009; and Cascadia, e.g., Han et al., 2017; Hyndman et al., 1993; MacKay, 1995, margins). How sediment is partitioned between the accretionary wedge and subducting plate becomes a critical factor, and that depends on where the décollement forms within the trench sedimentary section. In many thickly sedimented trenches, the décollement forms within the lower half of the trench section, possibly controlled by the presence of clay rich pelagic and hemipelagic sequences (Kopf, 2013). In contrast, along the entire ~1,000 km portion of the south central Chilean margin, the décollement forms at a shallow depth (Behrmann & Kopf, 2001; Geersen et al., 2011). As a consequence, frontal accretion of the trench sediment is limited, and 80–90% of the ~1.5 km thick sedimentary sequence in the trench is currently subducting beyond the lower slope (Olsen et al., 2020). This is consistent with a relatively small outer forearc (Bangs & Cande, 1997) compared to other settings that experience large earthquakes (e.g., Alaska, Moore et al., 1991; Nankai, Moore et al., 2009; Sumatra, Moeremans et al., 2014), most of which have large accretionary wedges and show significant frontal accretion. This characteristic of the south central Chilean margin ends abruptly near the northern edge of the slip in the 2010 Maule earthquake near −34.4°, north of which nearly all of the trench sediment is currently being accreted (Tréhu et al., 2019).

The differences between the south central Chilean margin and other thickly sedimented margins that host large tsunamigenic earthquakes raise the questions of how and why the Chilean margin behaves this way and how the outer forearc grows in the absence of significant frontal accretion. Furthermore, we can ask if these differences play a significant role in the occurrence of extraordinarily large megathrust earthquakes and, if so, how.

Until recently, the structure and processes across the outer Chilean forearc have proven very challenging to unravel (e.g., Bangs & Cande, 1997) due to difficulties with imaging the complex nature of the Chilean margin structure. In early 2017, we conducted the CEVICHE (Crustal Experiment from Valdivia to Illapel to Characterize Huge Earthquakes) seismic reflection survey to image the structure of the offshore Chilean forearc that ruptured in the *Mw* 8.3 Illapel, *Mw* 8.8 Maule, and *Mw* 9.5 Valdivia earthquakes. The primary goals of the survey were to investigate the geologic conditions that can cause such strong coupling and generate great earthquakes. In this paper, we present images of the margin structure across the region of largest slip during the Valdivia rupture. We focus on the structure within the outer 30–50 km of the forearc as imaged on four dip lines between Mocha and Chiloe Islands (Figure 1). The improved seismic data presented here reveal that the Chilean outer forearc wedge grows largely by irregular basal accretion rather than by more continuous frontal accretion, producing an outer wedge defined by distinctive internal structure. This process inhibits accretion and enables sediment subduction, which we also confirm from the images of deeply subducted sediment and the small volume of the outer wedge compared to the volume of sediment thought to have entered the trench since the latest phase of accretion began (possibly as recently as the Pliocene; Melnick & Echtler, 2006). In combination, these observations define a system wherein trench sediments are preferentially partitioned onto the downgoing plate and carried to depth. Consequently, the megathrust fault traverses a thick package of subducted sediments that serves to smooth the interface and separate the overlying basement units and underthrust rough igneous ocean crust. This configuration is sufficient to allow strong interseismic coupling and large megathrust earthquakes without developing an extensive accretionary wedge.

2. CEVICHE Seismic Profiles

During the 38 day CEVICHE data acquisition cruise on the R/V *Langseth*, we acquired nearly 5,000 km of very long source-receiver offset (15 km) 2-D seismic reflection data along 1,000 km of the south central Chilean margin (Figure 1).

The central Chilean margin is a remarkably complex structural setting in both strike and dip directions (e.g., Geersen et al., 2011). This makes it particularly challenging for 2-D seismic imaging by comparison to other thickly sedimented margins such as Nankai (Moore et al., 2009), Cascadia (Han et al., 2017), and Barbados (Westbrook, 1982). Seismic energy undergoes scattering and attenuation due to a combination of rough seafloor (Figure 1) and complex subseafloor deformational structures (e.g., Figure 2; see supporting information). Consequently, out-of-plane reflections, multiples, noise, and other artifacts degrade these images beyond what is typical for thickly sedimented subduction zones (e.g., Moeremans et al., 2014).

Processing of these data has proven to be particularly challenging due to very weak seismic returns from within the chaotic upper plate structure and strong seafloor multiples. We applied a low-cut filter (< 4 Hz) to suppress swell noise in shot gathers. Surface-related multiple elimination (SRME) was then applied on the shot gathers as a first step in multiple suppression. While SRME removed much of the multiple energy, the attempt to use radon transform techniques for further multiple suppression was unsuccessful because the signal below the multiple was too weak and too little primary signal remained after filtering. Instead, we applied LIFT multiple suppression (Choo et al., 2004) as the second step of multiple suppression. We relied on time-varying bandpass filtering to remove most of the remaining multiple with some loss of higher frequencies, particularly within deeper parts of the section. After applying normal moveout and mutes to remove excess stretching and multiples, we stacked and migrated the data. We applied Kirchhoff migration (both poststack and prestack; note that Figure 9 was produced with poststack time migration, but it excludes most of the data below the multiple) using a seawater velocity to collapse diffractions. We found that Kirchhoff migration with our data-derived velocity model created artifacts that obscured the weak signal too severely and smeared multiple energy throughout much of the section. Where the data were not obscured by multiples, migration with velocities appropriate for the subsurface did not improve the images substantially due to the presence of out-of-plane reflections and diffractions. The signal was further enhanced by applying trace mixing (nominally 13 traces, 162.5 m mixing window) to strengthen the coherent signal and f-k filtering (targeting dips of > ~4 ms/trace, > ~35°) to remove coherent dipping noise with parameters tailored to each individual line.

In spite of challenges, the long streamer, large seismic source and enhancements from processing described above have allowed us to image the deep structure of the margin more clearly than in previous studies (e.g., Bangs & Cande, 1997; Geersen et al., 2011). Here we present a structural interpretation of the four CEVICHE profiles that cross the region of greatest slip during the 1960 earthquake. We compare the seismic *P* wave velocity (V_p) derived from elastic full waveform inversion (FWI, Arnulf et al., 2014; Harding et al., 2016) of downward extrapolated long-offset streamer data (Arnulf et al., 2011, 2018) from Line 18 to the seismic reflectivity structure (Figure 3) (The FWI results will be presented in a separate publication). We also document the seismic reflection characteristics of three additional lines (Lines 16, 28, and 30) to identify structures that are typical for the margin across the high slip zone.

3. Structural Architecture of the Chilean Margin

In this section we present an overview of the structural architecture of the south central Chilean margin, before examining key elements in more detail. Figure 2 presents seismic Line 18 across the entire margin extending from the trench to the shelf, both in two-way traveltime and in depth, illustrating the primary structural elements. Structures are somewhat smoother and easier to interpret in the time section (Figure 2a) despite the geometric distortion resulting from the vertical axis being traveltime rather than depth. Figure 3 presents a preliminary velocity model for Line 18, clarifying some of the structural boundaries discussed below. Figure 4 presents the equivalent time section for Line 28 as an example of the southern pair of transects (Figure 1). The features described are interpreted in the context of those previously identified to the north and south of Line 18 (e.g., Contreras-Reyes et al., 2010).

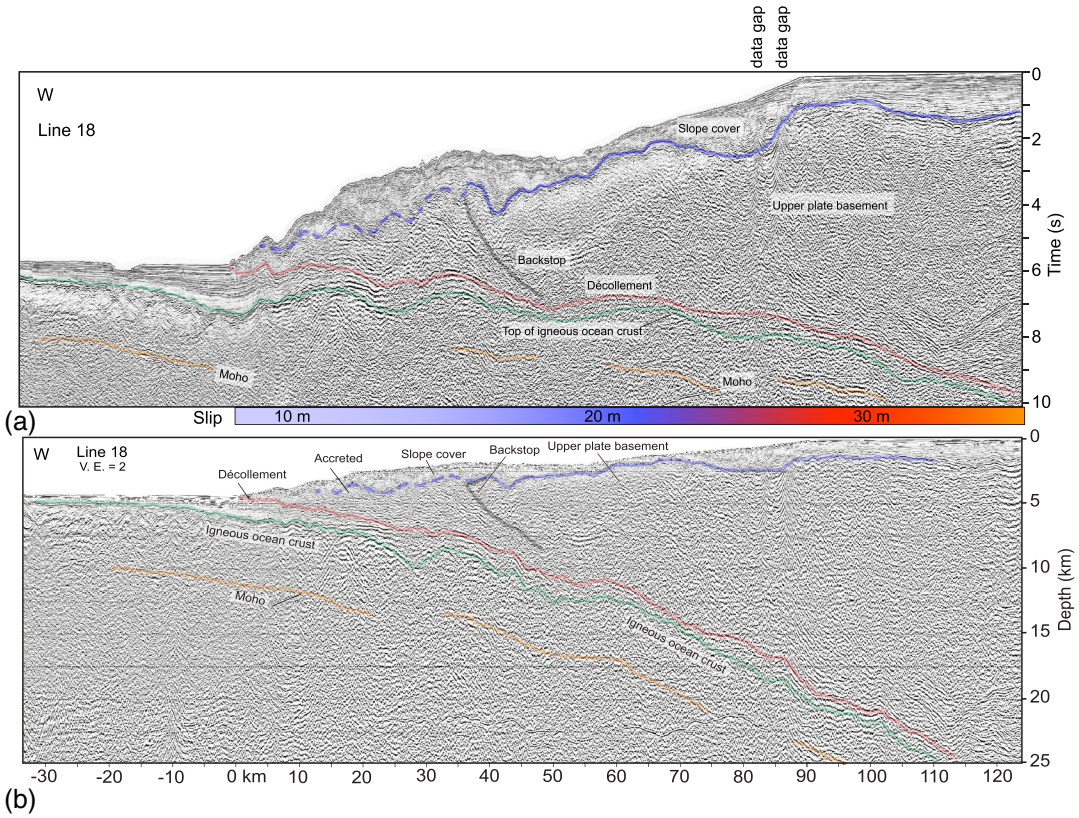

Figure 2. Interpreted seismic image of Line 18 from the CEVICHE seismic survey showing the Nazca plate ocean crust subducting from the trench to 25 km depth beneath the shelf. Location is shown in Figure 1. (a) Time section was migrated with a constant water velocity of 1.5 km/s to collapse seafloor diffractions and partially collapse subseafloor diffractions. See text for processing details. Shown are the base of the slope cover sediments (blue line), backstop separating the older accretionary wedge that forms the upper plate basement from the more recently accreted sediment (black line), the décollement that forms the megathrust slip surface (red line), the top of the subducting crust (green line), and Moho (orange line). Along the base of the profile is the slip estimate from the 1960 *Mw* 9.5 Valdivia earthquake as shown in Figure 1. (b) Depth section converted from the time section (shown in a) with velocities derived from streamer data and regional velocity models (Contreras-Reyes et al., 2010). Uninterpreted versions are shown in the supporting information.

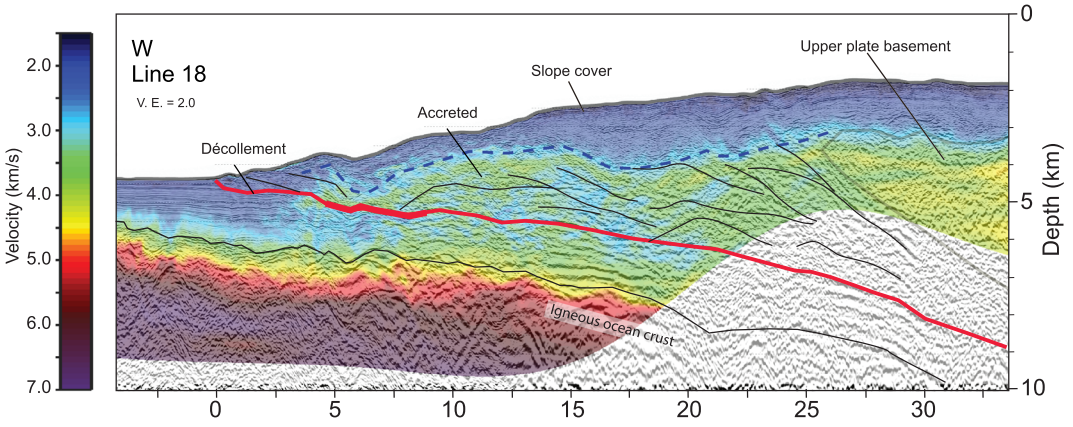

Figure 3. Seaward portion of seismic Line 18 shown in depth with overlying V_p results from full waveform inversion. The lines mark structures presented in Figure 2b. The thick segment of the decollement at ~7 km from the deformation front marks the largest contrast in velocity across the decollement. See text for details. An uninterpreted version is shown in the supporting information.

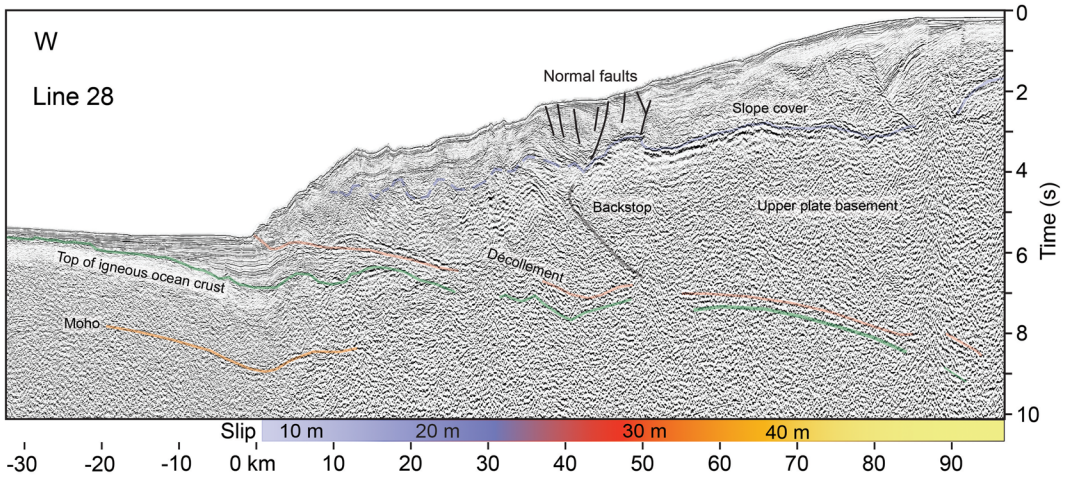

Figure 4. Interpreted seismic Line 28 from the CEVICHE survey (location shown in Figure 1). This time section was migrated with a constant water velocity of 1.5 km/s to collapse seafloor diffractions and partially collapse subseafloor diffractions. See text for processing details. Annotation is the same as for Figure 2. Along the base of the profile is the slip estimate from the 1960 *Mw* 9.5 Valdivia earthquake as shown in Figure 1. An uninterpreted version is shown in the supporting information.

On the northern transect (Line 18, Figure 2), we image a strong, but irregular, reflection across the profile that is consistent with the top of the subducting Nazca plate crust. We interpret this reflection as the top of igneous ocean crust (green line). Seaward of the deformation front, this interpretation of the top of the igneous ocean crust lies at the base of the horizontally stratified trench sediment wedge that is up to 1.5 km thick. We can trace this surface from the trench beneath the lower slope more or less continuously across the entire profile to approximately 25 km depth beneath the outer shelf. It is more difficult to discern beyond ~40–50 km from the trench, but it is still identifiable by spotty but prominent reflections. Beneath the trench, a parallel reflection lies 5–7 km below the top of ocean crust that we identify as Moho (orange line). This crustal thickness is typical for oceanic crust, which is ~26 Myr old here (Contreras-Reyes et al., 2010). Strong Moho reflections beneath the slope and shelf also lie at similar depths beneath the interpreted top of subducting crust basement and together help to confirm the interpretation of the top and bottom of Nazca plate igneous crust across the entire profile.

Deep within Line 18, we also image what appears to be the décollement distinctly above the oceanic crust. A series of discontinuous reflections lie roughly parallel to and 1–1.5 km above the top of the oceanic crust that we interpret as the décollement (red line), that is, the megathrust fault that slipped up to 40 m during the Valdivia earthquake (Barrientos & Ward, 1990; Moreno et al., 2009; Figures 1 and 2). This reflector is most pronounced within ~30–40 km of the trench, becoming less distinct with depth, where we identify it as the shallowest semicontinuous prominent reflector. The décollement does not generate a strong seismic reflection. We attribute the low amplitude of this seismic reflection at depth to the reduced differences in V_p across the boundary, as seen by the velocity model (note the change in contrast across the decollement at ~8 km from the trench marked by the thick line in Figure 3). The décollement defines the boundary between irregular seismic reflection patterns of the deformed accretionary wedge and the piece-wise laterally continuous strata capping the subducting plate. Several particularly strong reflections from underthrust sediment layers occur at ~20 km from the trench. The reflectors extend from the top of the igneous ocean crust to the base of the interpreted décollement, apparently preserving the original crustal onlapping patterns deposited in the trench basin. The interpreted thickness of the subducting trench sediment is ~1.5 km and is maintained to at least 40–50 km from the trench (Figure 2), at which point the two sets of bounding reflectors become discontinuous and more difficult to trace laterally. This consistency indicates that nearly all of the thick trench sediment sequence is subducted beyond the deformation front, as is typical for all of the south central Chilean margin (Olsen et al., 2020), but the results presented here extend the images of sediment subduction to much greater depth.

Within the shallow portions of the upper plate, a strong reflection lies 1–2 km below the seafloor and can be traced seaward from beneath the shelf to at least 35 km from the deformation front where it is a strong reflection on Line 18 (solid blue lines in Figure 2). (This surface likely extends as far seaward as ~10 km from the deformation front as shown by the blue dashed lines in Figure 2 based on additional criteria discussed further below). A similar reflection extends from the shelf edge to ~35–40 km on Line 28 (solid blue line in Figure 4). We interpret this horizon (the portion indicated by the solid blue line) to represent the boundary between stratified sedimentary sequences of Cretaceous age and younger overlying Paleozoic metamorphic basement, which was sampled by industry drill sites across the shelf near Isla Mocha and Chiloé (Gonzalez, 1990). The Paleozoic basement is believed to be the seaward extension of the Western Series Paleozoic accretionary complex exposed on land along this portion of Chile (Glodny et al., 2006). Older seismic refraction data (Contreras-Reyes et al., 2008) show that beneath the middle to upper slope, this reflection marks a large contrast in seismic velocity, with relatively low velocity slope cover sediments overlying moderate-velocity (4–5 km/s) crust, consistent with upper plate basement (Contreras-Reyes et al., 2010). The velocity contrast across this boundary is clearly evident in our velocity model as well (Figure 3). Contreras-Reyes et al. (2010) interpret the upper plate basement as an accretionary complex accreted before the Miocene, which extends to within 10–15 km of the deformation front and acts as a buttress, that is, a backstop, to the frontal accretionary wedge. Similarly, the prominent reflector is interpreted to delimit a resistant buttress on our profiles (Figures 2 and 4). The seaward edge of this basement unit is not well defined on our profiles, but landward dipping structures seaward of the backstop suggest that the basement also extends downward as a landward dipping boundary from the seaward edge of reflective upper boundary (gray, semitransparent line). This boundary may be the equivalent to the seaward edge of the paleo accretionary complex identified by Contreras-Reyes et al. (2008, 2010) to the north and south of Line 18 (near latitudes 38°S and 42°S), an interpretation supported by a lateral velocity contrast (black, semitransparent line in Figure 3). This older complex forming the backstop may have undergone extensive subduction erosion during the Miocene (Kukowski & Oncken, 2006; Melnick & Echtler, 2006), which could have truncated the seaward extent of this structure.

Across the lower slope and seaward of the interpreted backstop, the amplitude and continuity of the top of basement reflection decrease, denoting a change in the character, properties, and origin of the frontal wedge. A piece-wise continuous undulating interface can be identified reaching nearly to the trench (dashed blue line in Figures 2–4). The domain above this interface is distinguished by high-frequency, broadly continuous reflective horizons, locally distorted into coherent folds and contrasting dip domains and locally faulted. These are characteristics of slope sediments deposited on top of both the accreted strata and the basement unit. Their distorted appearance indicates complex deformation, punctuated by sedimentation and erosion, due to processes within the underlying rocks and/or by gravitationally driven deformation. In contrast, the underlying wedge is characterized by discordant packages of laterally continuous but spatially limited reflectors, generally oriented at low angles to the décollement, commonly but not exclusively dipping landward. These seismic characteristics suggest the presence of coherent stratal packages that have been disrupted, faulted and folded, that is, sediments accreted in front of the basement backstop. The character of the toe of the accretionary wedge is transitional between both the reflective frontal wedge and the shallow slope sediments, exhibiting high-frequency sedimentary reflections, locally folded and cut by faults. The seaward extension of the décollement beneath the wedge toe is clearly defined as the boundary between discordant reflective packages composing the subducting trench sediments and the deformed wedge. This accreted domain is discussed in more detail below, to better understand its origins.

The southern transect shows similar, equivalent structures across Line 28 (Figure 4). The seismic reflections interpreted as top of igneous ocean crust in Figure 4 are not as continuous as on Line 18, but they can be traced as a piece-wise continuous surface beneath the trench sediment section across the outer forearc to ~8 s two-way travel time (twtt) (~20 km), as on Line 18. There is also a piece-wise continuous reflection above the interpreted top of ocean crust across the profile to ~8 s depth. Based on its position above the interpreted ocean igneous crust, and because they track nearly parallel to it, we interpret this as the décollement. The inferred décollement reflection is also not as strong as on Line 18, but it is still recognizable above noise > ~0.5 s twtt (> ~1.0 km) above basement, as on Line 18. The lower strength of both reflections on Line 28 is partially due to the signal loss from the much stronger reflection interpreted as the top of the upper plate basement. The strong reflection from the top of upper plate basement has lower amplitude seaward of

~40 km from the deformation front and provides some of the basis for our interpretation of the seaward extent of the backstop along this profile. The slope cover sequences are also >1 km thick, similar to the northern transect, but here there are readily identifiable offsets in reflections interpreted as normal faults that indicate recent extension. Normal fault offset is small (less than a few tens of m) and does not appear to extend deeper than the slope cover sequences (Figure 4).

4. The Outer Forearc

A closer look at the outer forearc across four individual profiles (Figures 5–8) allows us to examine the structure between the trench and backstop in greater detail. We again focus on Line 18 (Figure 5) and Line 28 (Figure 6) because they exhibit some particularly clear structures within these two separate transects that guide our interpretation and can be compared to similar, but less distinct, structures on Lines 16 and 30, demonstrating consistency across the margin.

4.1. Trench Wedge and Décollement

Along Line 18 (Figures 2 and 5), we can trace reflections from the trench sediment strata continuously across the trench and beneath the deformation front and outer wedge. We note that there is very little sediment in layers parallel to and covering the roughness of the top of the oceanic igneous crust that would have been deposited on the igneous ocean crust prior to entering the trench. The trench sediments form a wedge that progressively onlaps the thin sediment layer on top of the oceanic igneous crust, or in some instances directly on the crust where the crust is elevated. These strata thicken and tilt landward as the oceanic crust bends into the trench, to reach a thickness of ~1.5 s (~2.0 km) at the deformation front. (See Figure 10 in Contreras-Reyes et al., 2010, and Figure 2 in Contreras-Reyes et al., 2007 for detailed views of the trench wedge geometry.) Beneath the lower slope, the well-defined trench fill reflectors terminate sequentially against the décollement fault, which thus defines a ramp cutting across the trench wedge. Small-offset faults appear to disrupt the trench fill immediately beneath the deformation front. These are interpreted to be protothrusts that are observed elsewhere along the margin (Olsen et al., 2020; Tréhu et al., 2019). Landward of the first ridge on this profile, the underthrust sediment reflectors are more difficult to follow, but they maintain the general pattern of seaward crustal onlap and landward termination against a prominent reflector interpreted as the active wedge décollement. A pair of strong reflections between 18 and 24 km on Line 18 further demonstrates that stratigraphic relationship.

Within the underthrust sediment, V_p increases from ~2.0 km/s in the trench to ~4.0 km/s with a patchy pattern of local velocity inversions, especially between 5 and 15 km from the deformation front (Figure 3). There is also a velocity inversion between the accretionary wedge and underthrust layer between 3 and 8 km from the deformation front (thick line in Figure 3), but farther landward this difference lessens and velocity inversions are more localized and patchier.

Line 28 (Figure 6) exhibits similar structural and stratigraphic relationships but with important differences. At the deformation front along the base of the lower slope, a series of four thrusts cut through the trench section, offsetting a distinct set of reflectors. The two frontal thrusts are steeply dipping and extend into the top approximately one third of the trench section (as shown in time). These two thrusts are ~500 m apart and have minimal offsets of < ~100 m and extend down to a common horizon. Deeper reflectors beneath this horizon terminate against the wedge décollement as observed on Line 18. This configuration demonstrates a change in décollement horizon, from a ramp propagating above the trench fill to a bedding parallel fault. The two frontal thrusts that ramp up from the tip of the bedding parallel décollement form a very small zone of frontal accretion on Line 28 (along with ~10 km long frontal ridges; Figure 1), uplifting an older structure that lies immediately landward. The small-offset faults on Line 18 (Figure 5) may represent an incipient stage of a similar episode of frontal accretion. Lines 30 and 16 (Figures 7 and 8) lack any evidence of such frontal accretion (nor do they have discernable frontal ridges; Figure 1; see supporting information); instead the décollement continues to track above the incoming trench fill.

Line 28 reveals another very distinct feature, which provides a clue to interpreting the structure of the outer forearc. At ~10 km landward of the deformation front, a prominent reflection (denoted by the red arrow in Figure 6) diverges from the underthrust reflections. The intervening reflections lap down onto the planar horizon below, a configuration best explained as folded trench fill strata overthrust upon a bedding

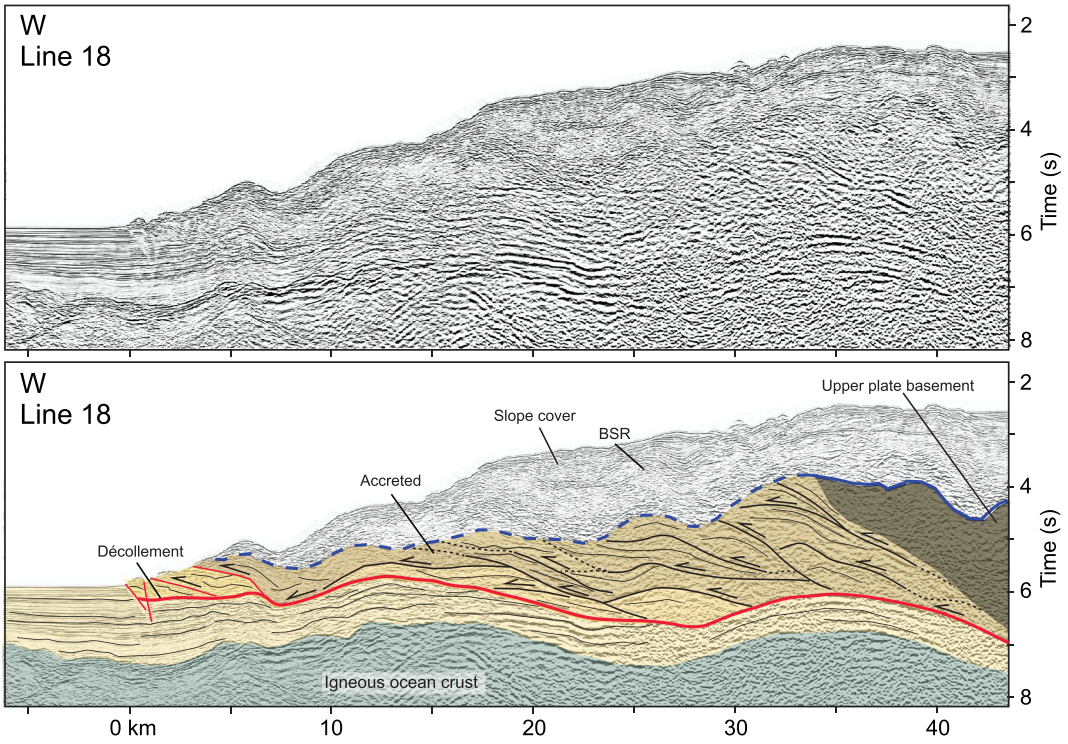

Figure 5. (top) Seaward portion of seismic Line 18 shown in two-way traveltime with automatic gain control and without annotation and interpretation. Location is shown in Figure 1. (bottom) Interpretation of Line 18. Yellow/brown shading shows trench sediments before subducting beneath the lower slope (left), subducted trench sediment (beneath décollement), and once accreted (above décollement and beneath slope cover). The boundary between accreted sediment and slope cover sediments is shown by blue dashed line. Faults within the accretionary wedge are interpreted as thrusts formed during underplating. Dark shading is the seaward extent of the upper plate basement that acts as a backstop to the outer wedge. See text for details.

parallel décollement fault. This strong reflection extends to 25 km, and the deeper underthrust layers pinch out downdip against the continuous reflection, consistent with the wedge décollement. This occurrence of folded trench strata at the base of the wedge can be explained by a similar shift in décollement horizon as noted at the toe of the wedge: a décollement that was initially overriding the trench sediments, branched downward onto a bedding parallel plane, and eventually ramped back up through the trench wedge, translating the thrust slice seaward with the upper plate. The thrust slice incorporates ~0.5 s thick section of sediment, about half of the underthrust section between 10 and 25 km from the deformation front. The fault at the top of the slice, its roof thrust, presumably was the original décollement before the slice was carved out but is no longer active. The fault at the base is the now active décollement.

The basal wedge structure described here is similar to structures along the Ecuador margin where they are interpreted to be slices of underplated sediment (Collot et al., 2011). Our interpretation is the same. We propose that the incorporation of this wedge-shaped thrust slice occurred beneath the wedge. The duplication of the trench sediments at depth also may have caused uplift of the upper plate, exaggerating the small seafloor ridge that lies directly above the deep fold. Examination of the seafloor bathymetry in this area (see supporting information) indicates that this ridge is a local feature, terminating near Line 28, and does not reach Line 30, ~12 km to the south. The deep structure described for Line 28 also does not appear on Line 30. We interpret that such underplated features do not extend very far along strike, even though they may define a primary mode of accretion in this setting.

4.2. Accretionary Wedge

The localized frontal accretion and duplication of strata at the base of the wedge on Line 28 (Figure 6) offer clues about the origins of the structures that form the rest of the outer forearc. Although best developed on Lines 18 and 28, the outer forearcs on all of the profiles (Figures 5–8) consist of packages of discontinuous

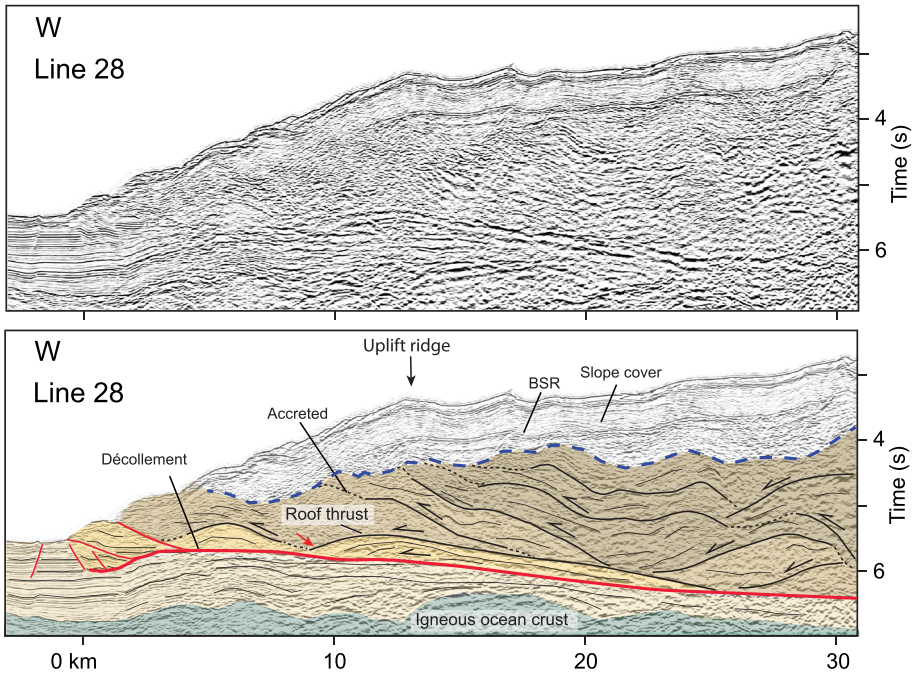

Figure 6. (top) Seaward portion of seismic Line 28 shown in two-way traveltime with automatic gain control and without annotation and interpretation. Location is shown in Figure 1. (bottom) Interpretation of Line 28. Yellow/brown shading shows trench sediments before subducting beneath the lower slope (left), subducted trench sediment (beneath décollement), and once accreted (above décollement and beneath slope cover). The boundary between accreted sediment and slope cover sediments is shown by blue dashed line. Faults within the accretionary wedge are interpreted as thrusts formed during underplating. See text for details.

bands of reflections (thin black lines) bounded by more prominent reflections that we interpret to be thrust faults (thicker black lines). The bounding thrusts stand out by changes in their dips and truncations of the intervening reflective bands. The continuity of the internal reflections indicates that some of these thrust packets are up to 10 km long and >1.0 s (1–1.5 km) thick. The deepest accreted domains extend the farthest seaward, with the shallower domains stepping, and often tilted, progressively landward. Small folds occur above the seaward terminations of some of bands (e.g., Line 18), with similar characteristics to folds found at the deformation front (Line 28).

The overall picture revealed on these profiles is an outer wedge constructed of stacks of accreted thrust sheets; however, the geometries differ from typical imbricate thrust stacks. Instead, the thrust sheets appear to have been peeled off of the downgoing strata and accreted to the base of the preexisting wedge, similar to the interpretation for the décollement structure described for Line 28 above. The >10 km lengths of each thrust sheet requires that the slices detached beneath the forearc, although the presence of preserved folds suggests that some of the sheets extended to the toe as well, where newly accreted frontal folds develop (Figure 5). As each thrust slice is incorporated into the overlying wedge, it uplifts and rotates the previously accreted sheets, causing the abandonment of older décollement strands that now define roof thrusts.

This model of progressive basal accretion is consistent with the seismic velocity patterns across the forearc on Line 18 (Figure 3). The accretionary wedge exhibits a patchy distribution of V_p values, ranging from >3.5 km/s near the top of the accreted section to ~2.5 km/s in the underlying section, indicating local inversions with depth throughout the accretionary wedge. The lower velocities at depth would correspond to the youngest and most recently accreted sedimentary packages. There are also lateral inversions. V_p at 15 km from the deformation front is lower than at 10 km. The patchiness and localized velocity inversions are consistent with the structural interpretation of irregularly stacked thrust sheets with significant overthrusting.

The accretionary wedges are capped by 1.0–1.5 s (~1 km) of slope cover sequences, interpreted based on the occurrence of higher frequency, parallel reflectors. The interpretation of these reflections is challenging in places, in particular, where reflections are obstructed by the prominent BSR ~1 s below the seafloor.

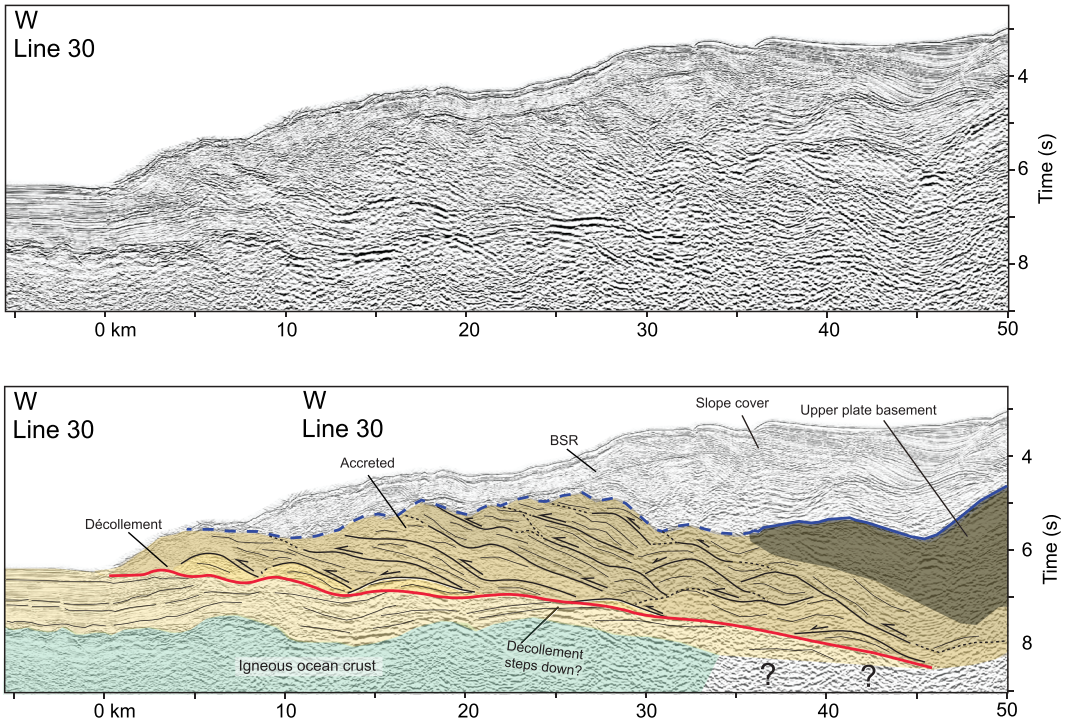

Figure 7. (top) Seaward portion of seismic Line 30 shown in two-way traveltime with automatic gain control and without annotation and interpretation. Location is shown in Figure 1. (bottom) Interpretation of Line 30. Yellow/brown shading shows trench sediments before subducting beneath the lower slope (left), subducted trench sediment (beneath décollement), and once accreted (above décollement and beneath slope cover). The boundary between accreted sediment and slope cover sediments is shown by blue dashed line. Faults within the accretionary wedge are interpreted as thrusts formed during underplating. Dark shading is the seaward extent of the upper plate basement that acts as a backstop to the outer wedge. See text for details.

However, the base of the slope cover (interpreted to be along the blue dashed lines in Figures 5–8) can be determined by changes in seismic character with depth and by distinctive contrasts in seismic velocity between the slope cover and accreted sediment (Figure 3). On all of the profiles, the slope cover exhibits broad folds with wavelengths of ~5–10 km, for example, between 20 and 30 km from the deformation front on Line 28 (Figure 6, and expanded view on Figure 9); similar features are also observed on Lines 16 and 30 (Figures 7 and 8). Many of these folds are conformable with underlying structure, including the folds identified at the seaward tips of the internal thrust sheets. However, the slope cover sequences also exhibit distinct packages of growth strata, unconformities and erosional surfaces (Figure 9). For example, at ~30 km from the deformation front on Line 28 (Figure 9), bedding layers steepen at depth, intensifying the corresponding fold. All of these features indicate syntectonic sedimentation consistent with ongoing uplift and subsidence within the underlying accretionary wedge.

4.3. The Wedge to Backstop Transition

The accreted section lies seaward of the upper plate basement that acts as a backstop to the accretionary wedge (dark shading in Figures 5, 7, and 8). In general, the boundary denotes a gradational lateral transition based on several characteristics. The basement lacks the laterally continuous reflections of the outer wedge, with some difficult to interpret exceptions (e.g., 45 km from the deformation front on Line 30). The slope cover landward of the interpreted backstop generally exhibits less internal deformation, with broader folds than found seaward of the backstop. This tendency is consistent with the presence of a stronger resistant zone, subject to less internal deformation. Concurrent with this decrease in deformation, seafloor roughness decreases landward (Figure 1; see supporting information). The amplitude of the reflection from the top of basement (most apparent on Lines 16 and 30; Figures 7 and 8) is very strong beneath the midslope area and decreases across the seaward extent of the interpreted backstop. As noted for Line 18, there is a moderate transition in V_p across this boundary from 4.0–4.5 km/s within the basement to 3.0–4.0 km/s seaward of

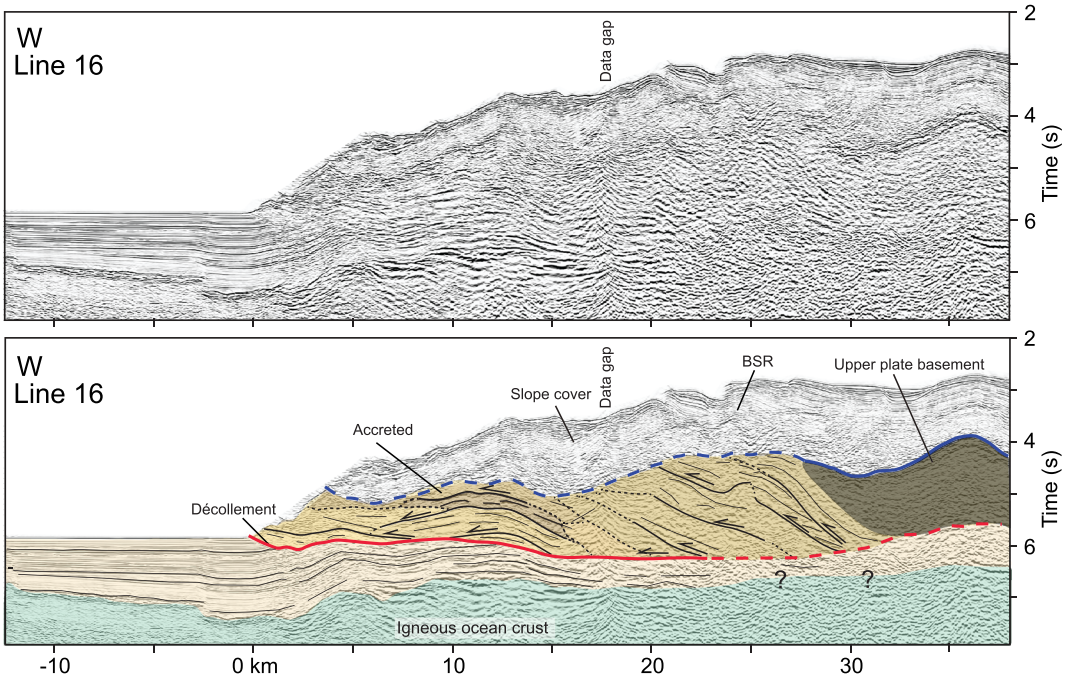

Figure 8. (top) Seaward portion of seismic Line 16 shown in two-way traveltime with automatic gain control and without annotation and interpretation. Location is shown in Figure 1. (bottom) Interpretation of Line 16. Yellow/brown shading shows trench sediments before subducting beneath the lower slope (left), subducted trench sediment (beneath décollement), and once accreted (above décollement and beneath slope cover). The boundary between accreted sediment and slope cover sediments is shown by blue dashed line. Faults within the accretionary wedge are interpreted as thrusts formed during underplating. Dark shading is the seaward extent of the upper plate basement that acts as a backstop to the outer wedge. See text for details.

the basement (Figure 3). Although modest, this velocity change further establishes a transition from the backstop to accretionary prism on this line.

5. Structure and Evolution of the Outer Forearc Along the Chilean Margin

The main features documented on the four seismic profiles presented provide constraints on the evolution of the margin. The common characteristics shown on all of the profiles include the following:

1. A primary décollement fault that separates well-stratified underthrust sediments from a more disrupted overriding wedge. This décollement extends all the way to the seafloor at the deformation front, ramping through or over the incoming trench fill strata, carrying the deformed wedge above it.
2. An outer accretionary wedge that has developed seaward of a transitional backstop, characterized by stacks of extensive thrust sheets, which exhibit a landward stair-stepping configuration, and progressively increasing landward dips. Small folds are evident at the seaward edges of some of these domains.
3. A draping cover of slope sediments often folded conformably with the underlying structures, with growth strata indicative of syntectonic sedimentation. No major faults cut through the slope sediments from the underlying wedge.

The details of these features vary among the lines as well. Lines 18 (Figure 5) and 28 (Figure 6) exhibit evidence for frontal accretion above branching décollements that cut into the underthrust sediment along bedding planes. In contrast, the frontal décollement on Lines 16 (Figure 8) and 30 (Figure 7) consistently cuts up through the trench section to the seafloor with little active frontal accretion. The orientations of the thrust sheets within the outer forearc also vary from line to line. Furthermore, none of the structures described are observed as along-strike continuations on nearby seismic lines, highlighting the along-strike variability and discontinuity and reflecting the irregular nature of accretion along the south central Chilean margin.

To evaluate the significance of the observed features, we first consider a steady state model for this margin in which the décollement position remains fixed. In this case, the décollement would propagate by ramping

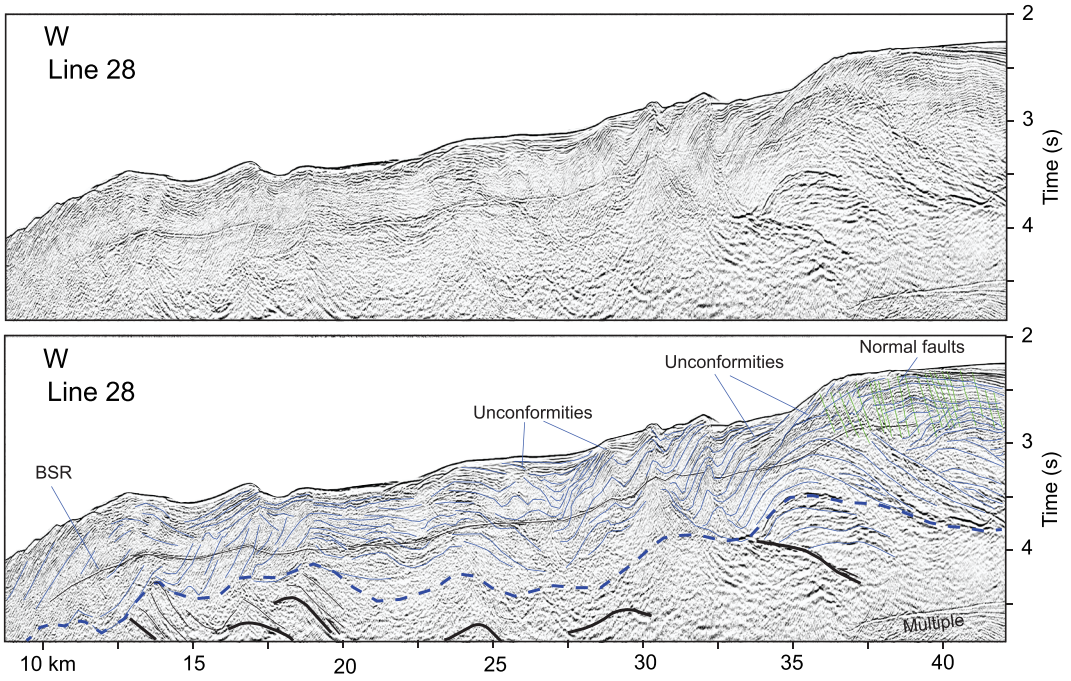

Figure 9. Line 28 fully migrated showing slope cover sequence in high resolution. The portion of the line shown here is indicated in Figure 1. The blue lines mark slope cover stratigraphy. The dashed line is the top of the accreted section. The black lines below the dashed line are accreted strata (thin) and thrust faults (thick). Green lines are normal faults. The data are displayed with automatic gain control to equalize amplitude with depth through the section.

through and overriding each new layer of sediment deposited in the trench, maintaining the distinct separation between the upper plate and subducting trench fill (solid red line indicating the décollement in Figure 10b). However, the four profiles presented here show that this is not always the case. The décollement fault is observed to branch downward along bedding horizons (dashed red line along the frontal zone of Figure 10b) in the seaward direction, a mechanism for frontal accretion of new trench sediments into the overriding wedge (Lines 18 and 28). But concurrently, branching and duplication of the décollement (solid and dashed red lines in Figure 10b) deep beneath the outer forearc, as observed on Line 28, demonstrate that accretion by underplating also occurs. The internal structure of the outer forearc thus suggests basal accretion of slices >10 km long of subducted trench sediments may also be a result of thrusts that initiated farther seaward during the development of frontal thrusts but were largely inactive until they engaged farther beneath the wedge. The combination of accretionary processes observed here suggests that a spectrum of behaviors occurs, ranging from frontal to basal accretion with a variety of scales.

The spectrum of accretionary behaviors appears to be controlled by three factors along the south central Chilean margin: (1) the lateral position where the décollement branches into the underlying strata, (2) the depth extent of the branching décollement, and (3) the relative activity of the décollement branch compared to the preexisting décollement (Figure 11). The ultimate outcome of the décollement branching responsible for frontal accretion on Lines 18 and 28, depends on the relative activity of the newly formed décollement branch compared to the preexisting décollement. If the original shallow décollement dominates, then the wedge will override the frontal faulted zone, effectively transporting the disrupted trench sediments to depth where they might eventually be underplated to the base of the wedge. Alternatively, if plate boundary slip transfers onto the deeper bedding plane fault, the trench fill will be frontally accreted to the toe of the overriding wedge. The narrow length of the trench strata will force the fault to divert upward and cut a new ramp to the seafloor. The thrust sheet carved from the sediments would overthrust the seafloor, extending the wedge seaward. In fact, both décollement branches may be active at different times, resulting in a complex alternation of deformation modes, including frontal accretion, basal underplating, and sediment subduction.

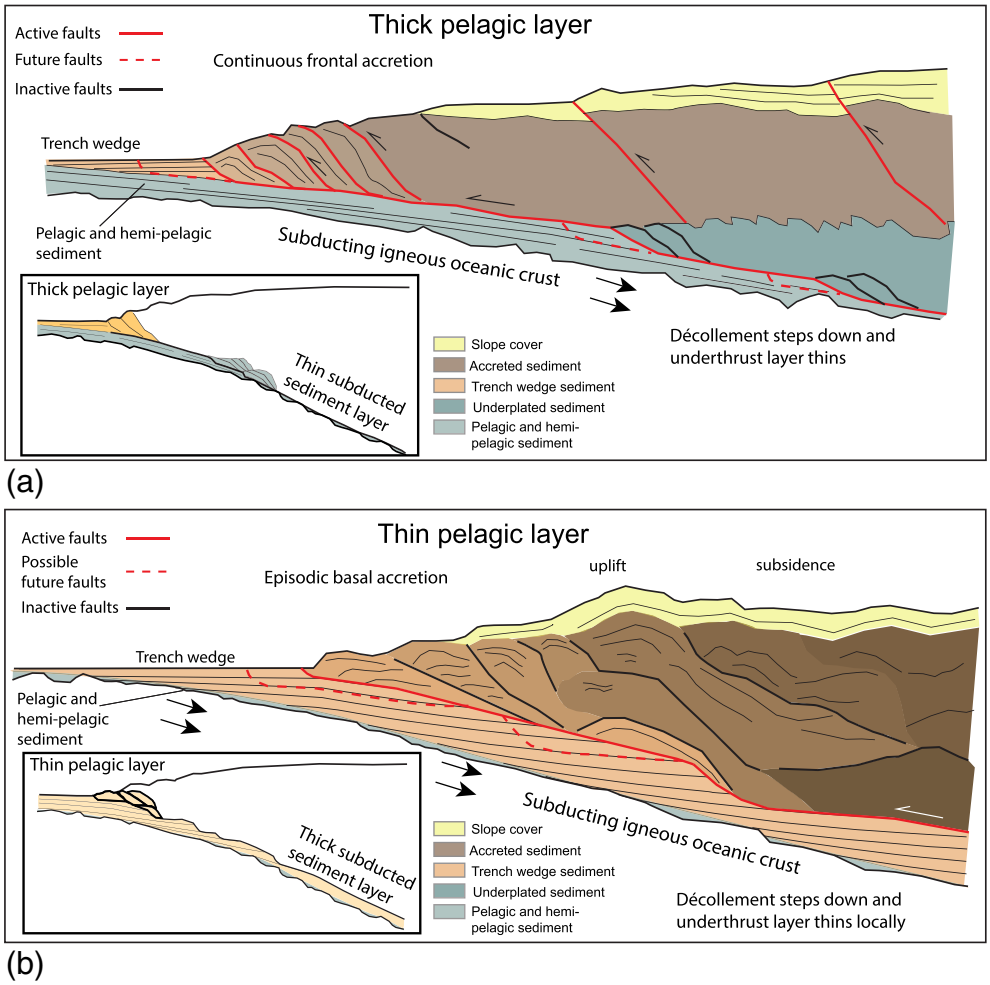

Figure 10. Models of outer forearcs in thickly sedimented subduction zones showing frontal and basal accretion structures and processes. (a) Model for subduction zones with thick pelagic and hemipelagic sediments on the incoming plate (after Moore & Vrolijk, 1992). Note that the décollement forms at a moderate level within the incoming trench section and regularly removes thrust slices that are imbricately stacked into the accretionary wedge. Thrust remains active as the wedge continues to grow. Deeper within the subduction zone, the décollement steps down to slip along deeper bedding planes and underplates sediment to the base of the wedge. (b) Our model for the south central Chile margin depicts a shallow décollement that forms near the top of the trench wedge sediment section and allows nearly all of the incoming sediment to subduct. Accretion occurs as the thrusts branch from the décollement into the trench wedge strata along bedding planes beneath the wedge (underplating) or into the undeformed trench wedge section (frontal accretion and underplating). Some branches may not persist (dashed red lines) or may reactivate beneath the wedge. Note that underplating removes sections and thins the underthrust strata, but thinning is localized and can return to its original thickness with further subduction.

We also see evidence for the initiation of décollement branching deeper beneath the outer forearc. Line 28 provides evidence for basal underplating beneath the wedge 10–25 km from the deformation front. On Line 18, prominent reflections beneath the décollement ~7 km landward from the deformation front suggest at least partial transfer of décollement slip onto a fault that follows a shallow bedding plane; a plane that extends across the trench to where it is close to the top of igneous ocean crust at the edge of the profile (Figures 2 and 5). Activation of this deeper fault may transfer shortening to the deformation front, where we see incipient protothrust faults in the underthrust package. The bounding structures define a 7 km long slice of underthrust sediments that thins landward. If the overlying décollement is abandoned, and slip continues on the deeper branch of the décollement, this thrust slice will eventually be basally accreted to the wedge, uplifting the overlying thrust sheets. If the frontal fold evident on this line is incorporated into the newly accreted slice, it will be preserved as a small fold at the seaward edges of the thrust sheets, similar

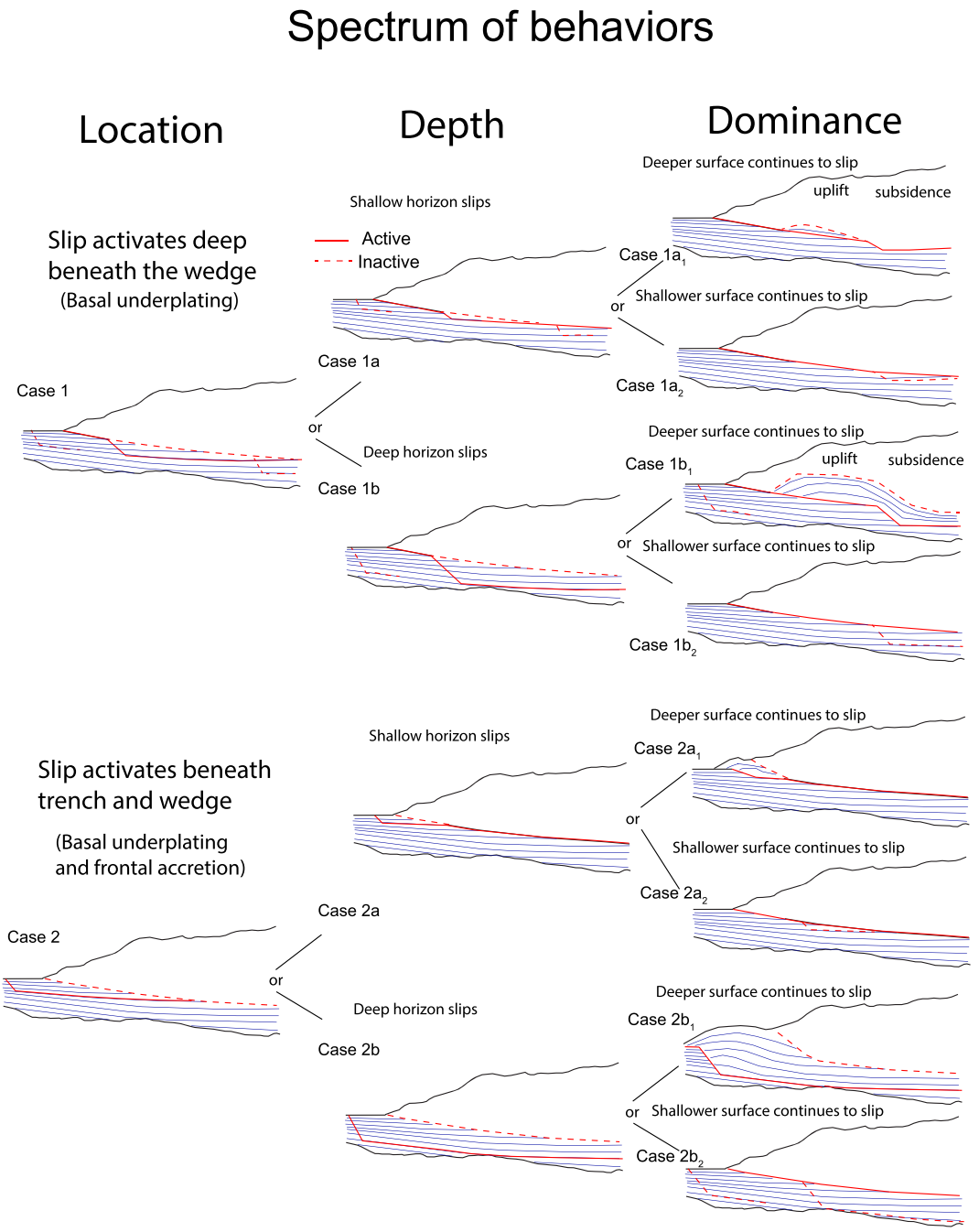

Figure 11. Models showing the spectrum of behaviors possible with the geometry of the frontal zone that is found along the south central Chile margin. The variables are the location within the outer forearc where the décollement branches, the depth to which the branch extends before it branches upward to the top of the underthrust sediment section, and the dominance between the newly formed branch and the preexisting décollement. Each of these behaviors are possible and may occur at different times depending on the trench wedge sediment properties and how they evolve with subduction beneath the outer forearc.

to those observed on many of the profiles (e.g., Lines 18 and 30). Incomplete underthrusting of such newly accreted thrust slices may account for the stair-stepping arrangement of the stacked thrust sheets and associated folds, similar to what is observed on Line 18. Thus, by this process, the wedge would grow both vertically and laterally.

As noted above, we see no evidence for recent thrust faults penetrating the slope cover. There are recognizable thrust faults that have several km of offset within the accretionary wedge, but none extend upward into the slope cover and have along-strike continuity of more than a few km (see supporting information). The lack of throughgoing thrust faults can be explained by persistent concentration of thrust activity at the base of the wedge during underplating. All of the shallower structures are passively uplifted in response without significant internal faulting. However, there is evidence for several small-offset normal faults in the midslope region (~40 km) of Line 28 (Figure 9). Such extensional features may result from differential uplift and folding during the vertical growth of the wedge. Thus, preexisting internal structures play no role in the continuous growth of the accretionary wedge in this location, in contrast to in-sequence and out-of-sequence thrusts present within margins dominated by frontal accretion (e.g., Nankai; Moore et al., 2009).

6. Discussion

6.1. The Unique Characteristics of the South Central Chilean Subduction Zone

The Chilean margin generates the world's largest earthquakes and tsunami, yet we do not understand what causes earthquakes in this setting to be particularly large. From empirical observations of global subduction zones, the thickness of sediment in the trench correlates with the settings that generate the largest earthquakes, leading to the prospect that megathrust earthquake settings subduct a sufficient amount of the trench sediment into the seismogenic zone to smooth the roughness of the subducting igneous ocean crust and the upper plate (Van Rijsingen et al., 2018). Although the Chilean margin meets the criterion of Scholl et al. (2015) with >1 km of sediment on the incoming plate, the 1.5–2.0 km of sediment in the Chilean trench is somewhat thin compared to other margins that produce great earthquakes, such as Sumatra (Dean et al., 2010), and it is not obvious that Chile should have particularly large earthquakes based on this mechanism alone. Furthermore, the trench sediment thickness is comparable to margins that produce smaller events such as Nankai (Ike et al., 2008) and the Aleutians (Li et al., 2018). These observations imply that either a substantially different mechanism controls great earthquakes along south central Chile, or unusual subduction processes allow particularly thick sediment subduction.

6.2. Unusual Structural Development Along the South Central Chilean Margin

There is substantial evidence of unusual structural development along south central Chile. The main structural features in our CEVICHE profiles that indicate fundamental differences distinct from other settings include the following:

1. Minimal, irregular frontal accretion;
2. Short along-strike continuity in protothrust ridges and seafloor uplift ridges;
3. Local downward branching of the décollement onto bedding planes within underthrust trench wedge strata beneath the accretionary wedge;
4. Intermittent basal accretion of underthrust sediments, underplating slices of trench sediments of variable thickness and length to the base of the accretionary wedge, concurrently uplifting and distorting the overriding plate.

These data collectively demonstrate a spectrum of possible structures that grow the outer forearc, by way of frontal accretion or underplating, and span hundreds to thousands of meters in thickness. The primary controls on the geometry and dimensions of the accreted slices of underthrust sediment appear to depend on the spacing of these décollement splays and their depth of penetration into the underthrust section. The ultimate emplacement of the thrust slices depends on the initial position of the décollement branch and/or the relative activity of the different fault branches. Figure 11 shows representative scenarios spanning this spectrum, which can explain the features that we see in the profiles presented here. Based on the interpreted structures of the outer forearcs (Figures 5–8), thin frontal and basal accretion (Cases 1a and 2a) is common and accretion of thick sections of the trench strata (Cases 1b and 2b) is rare. We hypothesize that décollement branching occurs preferentially at shallow depths, due to the presence of weaker, less lithified sediments or lower confining pressures. Similar factors may prevent the propagation of décollement branches down to the top of igneous ocean crust (Cases 1b and 2b), instead forcing the branches to cut back up section through the weaker shallow layers (Cases 1a and 2a). If this hypothesis is correct, it also implies that décollement branching is more likely to initiate near the deformation front (Case 2) but can remain inactive until it is carried

deeper along the main décollement where it is then activated during underplating. In other words, Case 1 is likely to initiate as Case 2, but whether it becomes Case 1 depends on which décollement surfaces are active. The mechanical conditions necessary to determine the relative activity between the décollement and the branches are critical to the process but currently unknown. All of these cases reflect an atypical partitioning of accreted and subducted sediment for thickly sedimented margins (Figure 10).

6.3. Unusually Thick Sediment Subduction Along the South Central Chilean Margin

The unusual structural development goes hand in hand with thick sediment subduction. Structural development along Chile contrasts with accretionary margins with thick sediment sections on the incoming plate that typically build large accretionary prisms by transferring the majority of the incoming sediment to the overriding plate (Moore & Vrolijk, 1992; Figure 10a). Along thickly sedimented trenches, the décollement usually forms within the lower half of the trench section, perhaps where high clay content within deep pelagic and hemipelagic sequences forms laterally extensive, weak layers conducive to development of a basal shear plane (Kopf, 2013). Consequently, sediment transfer by frontal accretion regularly removes 5–10 km long segments bounded by thrust faults that are continuous for many tens to hundreds of km along strike, forming imbricate stacks of sediment within the accretionary wedge (Figure 10a). Furthermore, some of the remaining subducted sediment along these margins may be underplated at depth as the décollement steps down to deeper layers that lie even closer to the top of the igneous ocean crust (Figure 10a). The general model for margins with thick incoming sediments is one with extensive frontal accretion and additional basal accretion that accretes most of the trench sediment and thins the subducted sediment layer as it builds a large accretionary wedge.

The Chilean margin differs substantially from this general model. Along the Chilean margin the décollement propagates into the trench section at a very shallow level (Figure 10b). The manifestation of this unusual behavior is two notable distinctions: (1) minimal frontal accretion and (2) transfer of most of the incoming sediments deep into the subduction zone.

The minimal frontal accretion and deep transfer of sediment is evident from mass balance calculations. In particular, the outer forearc seaward of the backstop is quite small relative to the volume of incoming sediment since the Early Pliocene (Bangs & Cande, 1997; Melnick & Echtler, 2006). The trench fill thickness has doubled within the past 25 Myr, which led to a major transition from erosion to accretion that began as early as the Middle Miocene (Kukowski & Oncken, 2006). From industry drilling and fission track data, Melnick and Echtler (2006) argue that accretion of the wedge seaward of the backstop along this segment of the margin began with the onset of Andean glaciation and erosion, which was first noted by Scholl et al. (1970), as late as the Early Pliocene. Currently, the interpreted volume of the wedge along Line 18, for example, is ~150 km^3 per km of the margin. Assuming a ~1.5 km thick underthrust trench section, this accounts for a minimum of ~100 km length of incoming sediments. Correcting for probable porosity reduction during accretion, for example, an average porosity of the trench sediment of ~30% (based on an average V_p of ~2.5 km/s) reduced to an average porosity of the wedge of ~20% (based on an average velocity of ~3.5 km/s), this yields closer to ~114 km of incoming sediments. The subduction rate over the last 5 Myr on average is ~80 km/Myr (DeMets et al., 2010), providing ~400 km of crust with the incoming sediment. This implies that, on average, ~30% of the incoming sediment was incorporated into the outer wedge, whereas ~70% was subducted beneath the upper plate backstop, and probably much deeper. Thus, the majority of the incoming sediment is subducted along this segment of the margin.

The deep reflections observed on our seismic lines are also consistent with the transfer of most of the incoming sediment deep within the Chilean subduction zone. The subducted sediment layer is sufficiently thick to produce two distinctly separate reflections from the décollement and the top of the subducting igneous ocean crust, as seen on both Lines 18 and 28. This differs from other settings, for example along the Alaska margin (Li et al., 2015), where only a single reflection is observed along the plate interface at equivalent depths. Significantly, the two reflections can be traced to at least 15 km depth below seafloor on Lines 18 and 28, and likely beyond, thus well within the highest slip regions of the Valdivia earthquake (Figure 2). Furthermore, U and ^{10}Be enrichment in arc volcano magmas, attributed to dehydration of trench sediment recently subducted to 100–150 km, also are particularly high in the vicinity of Lines 16/18 and Lines 28/30 (Sigmarsson et al., 1990), providing additional support for the large volumes of sediments subducted to great depth (deep enough for partial melting) in this area.

6.4. The Cause of These Unusual Subduction Processes Along the South Central Chilean Margin

The unusual structural development and tendency for sediment subduction are tied to spatial and temporal variations in décollement position, behavior, and activity, which forces a closer look at the nature of the incoming sedimentary section along the Chilean margin as a controlling factor in décollement position. What are its similarities or differences with other thickly sedimented subduction zones?

Along the Chilean continental margin, the pelagic and hemipelagic layers on the oceanic Nazca Plate seaward of the trench are quite thin, typically 100 to 200 m thick, and unable to continuously cover the igneous basement roughness (Contreras-Reyes et al., 2013; Völker et al., 2013). Once they are transported into the trench, these deeper strata lack laterally continuous bedding planes that can support laterally extensive décollement surfaces. Unlike the general model (Figure 10a), the trench wedge strata dominate the incoming sedimentary section. Furthermore, the trench wedge sediments accumulate within a narrow ~30–40 km wide basin along this segment of Chile (Figure 10b), which narrows due to greater plate bending north of 41°S (Contreras-Reyes et al., 2013). As the subducting plate bends toward the trench, the trench sediment layers tilt landward, developing the dipping sequence geometry that extends across the underthrust layers, as noted by others (e.g., Contreras-Reyes et al., 2010, 2013) and observed in our seismic profiles (Figure 10b).

The contrasting stratigraphic configurations described above may explain the different décollement behavior at the Chilean margin compared to other thickly sedimented margins. The absence of ocean crust-parallel pelagic and hemipelagic layers precludes the formation of laterally extensive continuous décollement surfaces. Instead, the décollement tracks the interface between the accreted wedge and the trench fill, only occasionally branching into a bedding plane within the trench sequence. But when that happens, the limited lengths of the bedding planes within the trench sequence and their orientations toward the base of the sediment section also restrict the downward extension of the décollement, forcing the fault to ramp back to the surface to maintain a continuous surface (Figure 10b). Thus, the unusual geometry and stratigraphy of the Chilean trench is likely a contributing factor to its tendency to form a shallow décollement that favors sediment subduction and inhibits systematic frontal accretion.

Décollement position is also influenced by the physical properties and lithologies of the trench sediments. Across the Barbados Ridge and Sumatra, seismic surveys and drilling deformation front show lithologic and physical property characteristics that lead to overpressures along weak layers within the incoming sediment conducive to seaward propagation of a continuous décollement (Dean et al., 2010; Deng & Underwood, 2001; Hüpers et al., 2017; Moore et al., 1998). In the Nankai trough, the décollement forms within with the deeper continuous sequences deposited seaward of the trench wedge and may be influenced more by lithology than high pore pressure (Kopf, 2013). Shallow drilling in the Chilean trench at Site 1232 (~60 km west of deformation front near 40°S) during IODP Leg 202, recovered Pleistocene turbidite layers of alternating thin sands and silts deposited during extensive Andean glaciation (Mix et al., 2003). Although this site is far from the deformation front and did not penetrate into layers that correlate directly with our seismic data in the trench, the drilling results do confirm the presence of extensive coarse-grained turbidites within the trench section, which are consistent with overbank deposits from axial channels diverted to the western trench basin by submarine canyon fans (Thornburg & Kulm, 1987). All four lines are located in between submarine canyons and at the distal edges of the canyon fans away from the transverse distributary fan channels (see supporting information; Thornburg & Kulm, 1987) and are likely reasonably equivalent depositional settings to the drill site. Olsen et al. (2020) present evidence that sand layers within these trench turbidites preserve permeable drainage pathways during rapid trench sedimentation. We speculate that the high permeability of these sediments prevents the buildup of significant overpressures, making the sediments relatively strong compared to other trench sections. As a result, the décollement will eschew the deep sediments and tend to localize within the shallow, high-porosity, weaker sediment near the top of the trench section, that is, at the interface between the accreted and underthrust domains, which favors a thick subducted sediment layer.

6.5. Implications for Great Earthquakes Along the South Central Chilean Margin

As argued by many, thick incoming sediments appear to be a key characteristic that correlates with the occurrence of great earthquakes (Heuret et al., 2012; Ruff, 1989; Scholl et al., 2015; van Rijsingen et al., 2018), and the Chilean margin clearly meets that essential criterion. However, many other features that are

associated with margins that host great earthquakes are not found here, in particular, a thick sedimentary section >200 m seaward of the trench, a laterally continuous, locally weak sedimentary horizon that the décollement occupies, and extensive frontal accretion that forms a large sedimentary accretionary prism. These elements appear to be associated with the formation of a laterally extensive, smooth megathrust fault interface that can support and release large shear stresses to generate great earthquakes. In contrast, the décollement along the Chilean margin frequently cross cuts strata and develops a locally weak shear zone at a shallow depth within the trench fill section, which allows most of the sediments that enter the subduction zone to be subducted. Consequently, a relatively small accretionary wedge develops above the décollement, and grows primarily by basal rather than frontal accretion. So, what are the conditions that allow great earthquakes to occur along this margin?

The primary condition appears to be preserving a thick enough underthrust package to isolate the décollement from the rough ocean crust topography, and for this condition to exist across an extensive region along the margin, both along strike and with depth. We estimate that ~1–1.5 km of sediment underlies the décollement down to depths of at least 15 km and possibly as deep as ~25 km or more. However, the thickness of the décollement zone is not known. We anticipate that near the toe and beneath the outer forearc, the décollement is relatively thin, possibly defined by a single fault strand 5–35 m thick (Rowe et al., 2013), well above the top of the igneous ocean crust. However, as these sediments are carried deeper into the subduction zone and subjected to higher stresses and more intense deformation, they are likely to become increasingly disrupted, undergoing fracturing, fragmentation, and comminution to form a thick zone of fault gouge and mélange (Kitamura et al., 2005; Rowe et al., 2013). Rowe et al. (2013) found that fault gouge and mélange thickness in drill cores and exhumed shear zones reached up to 350 m at 2 km depth but did not appear to increase further to depths of at least 15 km, likely due to weakness of the shear zone relative to the surrounding rocks. If this estimated thickness applies along the Chilean margin as well, the remaining 650–1,150 m thickness of underthrust sediments is still adequate to protect the décollement from interactions with preexisting ocean crust roughness. The separation between the megathrust and igneous ocean crust may also occur more easily here due to relatively smooth igneous ocean crust (Lallemand et al., 2018) and minimal faulting along plate-bending faults (Contreras-Reyes et al., 2007).

We recognize that underthrust layers at least 1 km thick are not unique to the Chilean margin (e.g., Bangs et al., 2009), but in many settings, these thick packages of sediment are interrupted by high relief subducting basement seamounts or ridges (e.g., Morgan & Bangs, 2017; Tréhu et al., 2012, 2019; von Huene et al., 2012), which may segment the margin seismically. However, along the Chilean margin the occurrence of a thick underthrust layer is persistent and widespread. It is the product of a narrow but deep trench that extends ~1,000 km along the margin, and experiences high rates of sedimentation accumulating a thick package of sediment capable of being subducted (Thornburg & Kulm, 1987). Furthermore, the preference for the décollement to localize at the interface between the trench sediments and the forearc ensures that most of these sediments are subducted. The combination of thick underthrust sediments and the shallow position of the décollement near the top of the underthrust section results in a laterally continuous shear zone that extends a significant distance both downdip and along strike without major obstructions. This configuration ensures the strong interseismic coupling necessary to produce large megathrust earthquakes along the south central Chilean margin.

7. Conclusion

New multichannel seismic reflection profiles acquired with a 15 km long streamer show that the south central Chilean margin has a very complex, irregular outer forearc structure that has grown in an unusual fashion by comparison with most other subduction zones.

Our results indicate the following:

1. The Chilean margin develops an unusual style of accretion that includes a spectrum of behaviors dominated by basal accretion. Accretion occurs irregularly when the décollement branches downward into the underthrust trench sediments in the seaward direction, following bedding planes that define new, deeper slip surfaces. This process leads to the underplating of trench sediments to the base of the upper plate. The spectrum of accretion behaviors depends on where décollement branches form, how deep they extend, and the relative slip displacement between existing and branching décollement surfaces.

2. The unusual accretionary style along south central Chile is a result of the geometry and lithologies of the incoming sediments. The pelagic and hemipelagic sections deposited seaward of the trench are very thin, <200 m, and do not cover igneous ocean crust relief, which prevents the development of a spatially extensive bedding plane slip surface for the décollement. Instead, the décollement localizes at the top of the trench fill wedge, only rarely stepping down into the wedge along a bedding horizon. Because of the narrow trench, bedding planes within the basin fill are not broadly continuous and instead onlap onto the top of subducting igneous crust in the seaward direction. Consequently, when décollement branching and underplating occur, the dimensions of the thrust sheets are constrained, limiting the volume of material that can be accreted.
3. The shallow position of the décollement and the unusual, irregular accretionary style results in subduction of a high fraction of the incoming sediment. The accretionary wedge developed since the Pliocene represents roughly 30% of all of the ~1.5 km thick incoming sediment section, which implies that, on average, a ~1 km thick sediment section is subducted beyond the upper plate backstop and into the areas of greatest locking and coseismic slip during the 1960 Valdivia earthquake. This thickness is consistent with the subducted sediment layer that we interpret from seismic reflections at depths >15 km.
4. The 1 km thick subducting sediment layer is sufficiently thick for a thick megathrust fault zone of mélange and fault gouge to form well above the top of igneous crust of the subducting oceanic plate. This separation allows for a continuous megathrust shear zone that is well above obstructions from the subducting igneous crust and forms a broad zone of strong coupling.
5. The mechanism that produces both the unusual, irregular accretionary wedge and allows thick sediment subduction is the result of the décollement interactions with the trench wedge sediment section. The lack of a pelagic and hemipelagic sediment section >200 m forces the décollement to interact with the trench wedge sediment. The thick trench wedge section is also common to all of the south central Chilean margin. This assures that this mechanism applies broadly, and a thick subducted sediment layer is inherent to this margin. It is the broad downdip and along-strike extent of this layer that also causes the strong plate coupling that leads to the extremely large megathrust earthquakes.

We believe that it is the atypical trench stratigraphy that is the primary cause for the unusual décollement behavior and, in turn, the unusual, complex accretionary structure. These conditions also enhance sediment subduction and allow strong coupling across a very broad megathrust, enabling unobstructed slip well above the top of the igneous ocean crust to generate the world's largest earthquakes.

Data Availability Statement

Data used in this study are publicly available from the Marine Geoscience Data System (http://www.marine-geo.org). This is UTIG Contribution Number 3705.

Acknowledgments

We would like to thank the captain, crew, and science party of the R/V *Marcus G. Langseth* for their help in collecting data for MGL1701. This work was supported by U.S. National Science Foundation grants OCE-1559293 and OCE-1558867. E. C.-R. acknowledges the support of the PIA-CONICYT, grant ACT172002. Seismic data processing and interpretation were completed using the Paradigm processing software packages Echos and Geodepth. We thank D. Scholl and R. von Huene for their help on an earlier version of this paper. We also thank M. Underwood and two annonymous reviewers for comments that greatly improved the manuscript.

References

Arnulf, A. F., Harding, A. J., Kent, G. M., & Wilcock, W. S. D. (2018). Structure, seismicity, and accretionary processes at the hot spot-influenced axial seamount on the Juan de Fuca Ridge. *Journal of Geophysical Research: Solid Earth*, *123*, 4618–4646. https://doi.org/10.1029/2017JB015131

Arnulf, A. F., Harding, A. J., Singh, S. C., Kent, G. M., & Crawford, W. C. (2014). Nature of upper crust beneath the Lucky Strike volcano using elastic full waveform inversion of streamer data. *Geophysical Journal International*, *196*(3), 1471–1491. https://doi.org/10.1093/gji/ggt461

Arnulf, A. F., Singh, S. C., Harding, A. J., Kent, G. M., & Crawford, W. (2011). Strong seismic heterogeneity in Layer 2A near hydrothermal vents at the mid-Atlantic ridge. *Geophysical Research Letters*, *38*, L13320. https://doi.org/10.1029/2011GL047753

Bangs, N. L., & Cande, S. C. (1997). Episodic development of a convergent margin inferred from structures and processes along the southern Chile margin. *Tectonics*, *16*(3), 489–503. https://doi.org/10.1029/97TC00494

Bangs, N. L. B., Moore, G. F., Gulick, S. P. S., Pangborn, E. M., Tobin, H. J., Kuramoto, S., & Taira, A. (2009). Broad, weak regions of the Nankai megathrust and implications for shallow coseismic slip. *Earth and Planetary Science Letters*, *284*(1), 44–49. https://doi.org/10.1016/j.epsl.2009.04.026

Barrientos, S. E., & Ward, S. N. (1990). The 1960 Chile earthquake: Inversion for slip distribution from surface deformation. *Geophysical Journal International*, *103*(3), 589–598. https://doi.org/10.1111/j.1365-246X.1990.tb05673.x

Behrmann, J. H., & Kopf, A. (2001). Balance of tectonically accreted and subducted sediment at the Chile triple junction. *International Journal of Earth Sciences*, *90*(4), 753–768. https://doi.org/10.1007/s005310000172

Choo, J., Downton, J., & Dewar, J. (2004). LIFT: A new and practical approach to noise and multiple attenuation. *First Break*, *22*, 39–44. https://doi.org/10.3997/1365-2397.2004009

Cifuentes, I. L. (1989). The 1960 Chilean earthquakes. *Journal of Geophysical Research*, *94*(B1), 665–680. https://doi.org/10.1029/JB094iB01p00665

Cisternas, M., Atwater, B. F., Torrejón, F., Sawai, Y., Machuca, G., Lagos, M., & Shishikura, M. (2005). Predecessors of the giant 1960 Chile earthquake. *Nature*, *437*(7057), 404–407. https://doi.org/10.1038/nature03943

Collot, J. Y., Ribodetti, A., Agudelo, W., & Sage, F. (2011). The south Ecuador subduction channel: Evidence for a dynamic mega-shear zone from 2D fine-scale seismic reflection imaging and implications for material transfer. *Journal of Geophysical Research*, *116*, B11102. https://doi.org/10.1029/2011JB008429

Contreras-Reyes, E., & Carrizo, D. (2011). Control of high oceanic features and subduction channel on earthquake ruptures along the Chile–Peru subduction zone. *Physics of the Earth and Planetary Interiors*, *186*(1–2), 49–58. https://doi.org/10.1016/j.pepi.2011.03.002

Contreras-Reyes, E., Flueh, E. R., & Grevemeyer, I. (2010). Tectonic control on sediment accretion and subduction off south-central Chile: Implications for coseismic rupture processes of the 1960 and 2010 megathrust earthquakes. *Tectonics*, *29*, TC6018. https://doi.org/10.1029/2010TC002734

Contreras-Reyes, E., Grevemeyer, I., Flueh, E. R., & Reichert, C. (2008). Upper lithospheric structure of the subduction zone offshore of southern Arauco peninsula, Chile, at 38°S. *Journal of Geophysical Research*, *113*, B07303. https://doi.org/10.1029/2007JB00556

Contreras-Reyes, E., Grevemeyer, I., Flueh, E. R., Scherwath, M., & Heesemann, M. (2007). Alteration of the subducting oceanic lithosphere at the southern Central Chile trench–outer rise. *Geochemistry, Geophysics, Geosystems*, *8*, Q07003. https://doi.org/10.1029/2007GC001632

Contreras-Reyes, E., Jara, J., Maksymowicz, A., & Weinrebe, W. (2013). Sediment loading at the southern Chilean trench and its tectonic implications. *Journal of Geodynamics*, *66*, 134–145. https://doi.org/10.1016/j.jog.2013.02.009

Dean, S. M., McNeill, L. C., Henstock, T. J., Bull, J. M., Gulick, S. P. S., Austin, J. A., et al. (2010). Contrasting décollement and prism properties over the Sumatra 2004/2005 earthquake rupture boundary. *Science*, *329*(5988), 207–210. https://doi.org/10.1126/science.1189373

DeMets, C., Gordon, R. G., & Argus, D. F. (2010). Geologically current plate motions. *Geophysical Journal International*, *181*(1), 1–80. https://doi.org/10.1111/j.1365-246X.2009.04491.x

Deng, X., & Underwood, M. B. (2001). Abundance of smectite and the location of a plate-boundary fault, Barbados accretionary prism. *Geological Society of America Bulletin*, *113*, 495–507. https://doi.org/10.1130/0016-7606(2001)113<0495:AOSATL>2.0CO;2

Geersen, J., Behrmann, J. H., Völker, D., Krastel, S., Ranero, C. R., Diaz-Naveas, J., & Weinrebe, W. (2011). Active tectonics of the south Chilean marine forearc (35°S–40°S). *Tectonics*, 16, TC3006. https://doi.org/10.1029/2010TC002777

Glodny, J., Echtler, H., Figueroa, O., Pranz, G., Grafe, K., Kemnitz, H., et al. (2006). Long-term geological evolution and mass-flow balance of the south-central Andes. In O. Onken et al. (Eds.), *The Andes: Active subduction orogeny, frontiers in Earth sciences* (Vol. 3, pp. 401–428). Berlin-Heidelberg-New York: Springer.

Gonzalez, E. (1990). Hydrocarbon resources in the coastal zone of Chile. In G. E. Ericksen, M. T. Canas Pinochet, J. A. Reinemund (Eds.), *Geology of the Andes and its relation to hydrocarbon and mineral resources*, *Circum-Pacific Council for Energy and Mineral Resources Earth Science Series* (Vol. 11, pp. 383–404). Houston, Texas: Circum-Pacific Council for Energy and Mineral Resources.

Han, S., Bangs, N. L., Carbotte, S. M., Saffer, D. M., & Gibson, J. C. (2017). Variations in sediment consolidation along the Cascadia margin determine forearc deformation and megathrust slip behavior. *Nature Geoscience*, *10*(12), 954–959. https://doi.org/10.1038/s41561-017-0007-2

Harding, A. J., Arnulf, A., & Blackman, D. (2016). Velocity structure near IODP Hole U1309D, Atlantis Massif, from waveform inversion of streamer data and borehole measurements. *Geochemistry, Geophysics, Geosystems*, *17*, 1990–2014. https://doi.org/10.1002/2016GC006312

Heuret, A., Conrad, C. P., Funiciello, F., Lallemand, S., & Sandri, L. (2012). Relation between subduction megathrust earthquakes, trench sediment thickness and upper plate strain. *Geophysical Research Letters*, *39*, L05304. https://doi.org/10.1029/2011GL050712

Hüpers, A., Torres, M. E., Owari, S., McNeill, L. C., Dugan, B., Henstock, T. J., et al. (2017). Release of mineral-bound water prior to subduction tied to shallow seismogenic slip off Sumatra. *Science*, 841–844. https://doi.org/10.1126/science.aal3429

Hyndman, R. D., Wang, K., Yuan, T., & Spence, G. D. (1993). Tectonic sediment thickening: Fluid expulsion and the thermal regime of subduction zone accretionary prisms: The Cascadia margin off Vancouver Island. *Journal of Geophysical Research*, *98*(B12), 21,865–21,876. https://doi.org/10.1029/93JB02391

Ike, T., Moore, G. F., Kuramoto, S., Park, J.-O., Kaneda, Y., & Taira, A. (2008). Variations in sediment thickness and type along the northern Philippine Sea plate at the Nankai trough. *Island Arc*, *17*(3), 342–357. https://doi.org/10.1111/j.1440-1738.2008.00624.x

Kitamura, Y., Sato, K., Ikesawa, E., Ikehara-Ohmori, K., Kimura, G., Kondo, H., et al. (2005). Mélange and its seismogenic roof décollement: A plate boundary fault rock in the subduction zone—An example from the Shimanto Belt Japan. *Tectonics*, *24*, TC5012. https://doi.org/10.1029/2004TC001635

Kopf, A. (2013). Effective strength of incoming sediments and its implications for plate boundary propagation: Nankai and Costa Rica as type examples of accreting vs. erosive convergent margins. *Tectonophysics*, *608*, 958–969. https://doi.org/10.1016/j.tecto.2013.07.023

Kukowski, N., & Oncken, O. (2006). Subduction erosion: The "normal" mode of forearc material transfer along the Chilean margin? In O. Onken et al. (Eds.), *The Andes: Active subduction orogeny, frontiers in Earth sciences* (Vol. 3, pp. 217–236). Berlin-Heidelberg-New York: Springer.

Lallemand, S., Peyret, M., van Rijsingen, E., Arcay, D., & Heuret, A. (2018). Roughness characteristics of oceanic seafloor prior to subduction in relation to the seismogenic potential of subduction zones. *Geochemistry, Geophysics, Geosystems*, *19*, 2121–2146. https://doi.org/10.1029/2018GC007434

Li, J., Shillington, D. J., Bécel, A., Nedimovic, M. R., Webb, S. C., Saffer, D. M., et al. (2015). Downdip variations in seismic reflection character: Implications for fault structure and seismogenic behavior in the Alaska subduction zone. *Journal of Geophysical Research: Solid Earth*, *120*, 7883–7904. https://doi.org/10.1002/2015JB012338

Li, J., Shillington, D. J., Saffer, D. M., Bécel, A., Nedimovic, M. R., Webb, S. C., et al. (2018). Connections between subducted sediment, pore-fluid pressure, and earthquake behavior along the Alaska megathrust. *Geology*, *46*(4), 299–302. https://doi.org/10.1130/G39557.1

MacKay, M. E. (1995). Structural variation and landward vergence at the toe of the Oregon accretionary prism. *Tectonics*, *14*, 1309–1320. https://doi.org/10.1029/95TC02320

Melnick, D., Bookhagen, B., Strecker, M. R., & Echtler, H. P. (2009). Segmentation of megathrust rupture zones from fore-arc deformation patterns over hundreds to millions of years, Arauco Peninsula, Chile. *Journal of Geophysical Research*, *114*, B01407. https://doi.org/10.1029/2008JB005788

Melnick, D., & Echtler, H. P. (2006). Inversion of forearc basins in south-central Chile caused by rapid glacial age trench fill. *Geology*, *34*, 709–712. https://doi.org/10.1130/G22440.1

Mix, A. C., Tiedemann, R., & Blum, P. (2003). *Proc. ODP, Init. Repts., 202*. College Station, TX: Ocean Drilling Program. https://doi.org/10.2973/odp.proc.ir.202.2003

Moeremans, R., Singh, S. C., Mukti, M., Mcardle, J., & Johansen, K. (2014). Seismic images of structural variations along the deformation front of the Andaman–Sumatra subduction zone: Implications for rupture propagation and tsunamigenesis. *Earth and Planetary Science Letters*, *386*(1), 75–85. https://doi.org/10.1016/j.epsl.2013.11.003

Moore, C. J., Diebold, J., Fisher, M. A., Sample, J., Brocher, T., Talwani, M., et al. (1991). EDGE deep seismic reflection transect of the eastern Aleutian arc-trench layered lower crust reveals underplating and continental growth. *Geology*, *19*(5), 420–424. https://doi.org/10.1130/0091-7613(1991)019<0420:EDSRTO>2.3.CO;2

Moore, G. F., Park, J.-O., Bangs, N. L., Gulick, S. P., Tobin, H. J., Nakamura, Y., et al. (2009). Structural and seismic stratigraphic framework of the NanTroSEIZE Stage 1 transect. In M. Kinoshita et al. (Eds.), *The Expedition 314/315/316 scientists, Proc. IODP,* 314/315/316 (pp. 1–46). College Station, TX: Ocean Drilling Program. https://doi.org/10.2204/iodp.proc.314315316.102.2009

Moore, J., & Vrolijk, P. (1992). Fluids in accretionary prisms. *Reviews of Geophysics*, *30*(2), 113–135. https://doi.org/10.1029/92RG00201

Moore, J. C., Klaus, A., Bangs, N. L., Bekins, B. A., Buecker, C. J., Brueckmann, W., et al. (1998). Consolidation patterns during initiation and evolution of a plate-boundary décollement zone; northern Barbados accretionary prism. *Geology*, *26*, 811–814. https://doi.org/10.1130/0091-7613(1998)026<0811:cpdiae>2.3.co;2

Moreno, M., Melnick, D., Rosenau, M., Baez, J., Klotz, J., Oncken, O., et al. (2012). Toward understanding tectonic control on the M_w 8.8 2010 Maule Chile earthquake. *Earth and Planetary Science Letters*, *321–322*, 152–165. https://doi.org/10.1016/j.epsl.2012.01.006

Moreno, M. S., Bolte, J., Klotz, J., & Melnick, D. (2009). Impact of megathrust geometry on inversion of coseismic slip from geodetic data: Application to the 1960 Chile earthquake. *Geophysical Research Letters*, *36*, L16310. https://doi.org/10.1029/2009GL039276

Morgan, J. K., & Bangs, N. L. (2017). Recognizing seamount-forearc collisions at accretionary margins: Insights from discrete numerical simulations. *Geology*, *45*(7), 635–638. https://doi.org/10.1130/G38923.1

Olsen, K. M., Bangs, N. L., Tréhu, A. M., Han, S., Arnulf, A., & Contreras-Reyes, E. (2020). Thick, strong sediment subduction along south-central Chile and its role in great earthquakes. *Earth and Planetary Science Letters*, *538*, 116195. https://doi.org/10.1016/j.epsl.2020.116195

Rowe, C. D., Moore, J. C., Remitti, F., & the IODP Expedition 343/343T Scientists (2013). The thickness of subduction plate boundary faults from the seafloor into the seismogenic zone. *Geology*, *41*(9), 991–994. https://doi.org/10.1130/G34556.1

Ruff, L. J. (1989). *Do trench sediments affect great earthquake occurrence in subduction zones? PAGEOPH 129: 263.* Basel Switzerland. https://doi.org/10.1007/BF00874629

Scholl, D. W., Christensen, M. N., von Huene, R., & Marlow, M. S. (1970). Peru-Chile trench sediments and sea floor spreading. *Geological Society of America Bulletin*, *81*(5), 1339–1360. https://doi.org/10.1130/0016-7606(1970)81[1339:PTSASS]2.0.CO;2

Scholl, D. W., Kirby, S. H., von Huene, R., Ryan, H., Wells, R. E., & Geist, E. L. (2015). Great ($\geq M_w$8.0) megathrust earthquakes and the subduction of excess sediment and bathymetrically smooth seafloor. *Geosphere*, *11*, 236–265. https://doi.org/10.1130/GES01079.1

Seno, T. (2017). Subducted sediment thickness and M_W 9 earthquakes. *Journal of Geophysical Research: Solid Earth*, *122*, 470–491. https://doi.org/10.1002/2016JB013048

Sigmarsson, O., Condomines, M., Morris, J. D., & Harmon, R. S. (1990). Uranium and ^{10}Be enrichments by fluids in Andean arc magmas. *Nature*, *346*, 163–165. https://doi.org/10.1038/346163a0

Thornburg, T. M., & Kulm, L. D. (1987). Sedimentation in the Chile trench: Depositional morphologies, lithofacies, and stratigraphy. *Geological Society of America Bulletin*, *98*(1), 33–52. https://doi.org/10.1130/0016-7606(1987)98<33:SITCTD>2.0.CO;2

Tréhu, A. M., Blakely, R. J., & Williams, M. C. (2012). Subducted seamounts and recent earthquakes beneath the central Cascadia forearc. *Geology*, *40*, 103–106. https://doi.org/10.1130/G32460.1

Tréhu, A. M., Hass, B., de Moor, A., Maksymowicz, A., Contreras-Reyes, E., Vera, E., & Tryon, M. (2019). Geologic controls on up-dip and along-strike propagation of slip during subduction zone earthquakes from a high-resolution seismic reflection survey across the northern limit of slip during the 2010 M_w8.8 Maule earthquake. *Geosphere*, *15*, 1751–1773. https://doi.org/10.1130/GES02099.1

van Rijsingen, E., Lallemand, S., Peyret, M., Arcay, D., Heuret, A., Funiciello, F., & Corbi, F. (2018). How subduction interface roughness influences the occurrence of large interplate earthquakes. *Geochemistry, Geophysics, Geosystems*, *19*, 2342–2370. https://doi.org/10.1029/2018GC007618

Völker, D., Geersen, J. M., Contreras-Reyes, E., & Reichert, C. (2013). Sedimentary fill of the Chile trench (32–46°S): Volumetric distribution and causal factors. *Journal of the Geological Society*, *170*(5), 723–736. https://doi.org/10.1144/jgs2012-119

von Huene, R., Miller, J. J., & Weinrebe, W. (2012). Subducting plate geology in three great earthquake ruptures of the western Alaska margin, Kodiak to Unimak. *Geosphere*, *8*(3), 628–644. https://doi.org/10.1130/GES00715.1

Wang, K., & Bilek, S. L. (2011). Do subducting seamounts generate or stop large earthquakes? *Geology*, *39*, 819–822. https://doi.org/10.1130/G31856.1

Westbrook, G. K. (1982). The Barbados ridge complex: Tectonics of a mature forearc system. *Geological Society, London, Special Publications*, *10*(1), 275–290. https://doi.org/10.1144/GSL.SP.1982.010.01.18